Journal of the Endocrine Society, 2022, **6**, 1–8
https://doi.org/10.1210/jendso/bvac126
Advance access publication 15 August 2022
Clinical Research Article

Adrenal Near-Infrared Autofluorescence

Neel Rajan,[2,*] Steven D. Scoville,[1,*] Tong Zhang,[3] Priya H. Dedhia,[4] Barbra S. Miller,[4] Matthew D. Ringel,[2] Abberly Lott Limbach,[5] and John E. Phay[4]

[1]Department of Surgery, The Ohio State University Wexner Medical Center, Columbus, Ohio 43210, USA
[2]Division of Endocrinology, Diabetes, and Metabolism, Department of Medicine, The Ohio State University Wexner Medical Center, Columbus, Ohio 43210, USA
[3]Campus Microscopy and Imaging Facility, The Ohio State University, Columbus, Ohio 43210, USA
[4]Division of Surgical Oncology, Department of Surgery, The Ohio State University Wexner Medical Center, Columbus, Ohio 43210, USA; and
[5]Department of Pathology, The Ohio State University Wexner Medical Center, Columbus, Ohio 43210, USA

*These authors contributed equally to this work.
Correspondence: John E. Phay, MD, Division of Surgical Oncology, Department of Surgery, The Ohio State University Wexner Medical Center, 410 W 10th Ave, Columbus, OH 43210, USA. Email: John.Phay@osumc.edu.

Abstract

Context: Parathyroid tissue is one of the few tissues to have strong near-infrared (NIR) autofluorescence, which has been exploited to improve intraoperative parathyroid identification. The US Food and Drug Administration has approved 2 devices for this purpose. Adrenal glands can be difficult to distinguish from surrounding fat, an issue during total adrenalectomy.

Objective: We hypothesized adrenal tissue may also possess considerable NIR autofluorescence.

Methods: Resected patient adrenal specimens were examined after robotic adrenalectomy with an NIR camera intraoperatively. Patients did not receive fluorescent dye. Images were taken of both gross and sectioned specimens. Post hoc image analysis was performed with ImageJ software. Confocal microscopy was performed on selected tissues using immunofluorescence and hematoxylin-eosin staining.

Results: Resected tissue was examined from 22 patients undergoing surgery for pheochromocytomas (6), primary aldosteronism (3), adrenocorticotropin-independent hypercortisolism (10), and a growing or suspicious mass (3). Normal adrenal tissue demonstrated strong NIR autofluorescence. The intensity ratio compared to background (set as 1) for gross images was 2.03 ± 0.51 ($P < .0001$) compared to adjacent adipose of 1.24 ± 0.18. Autofluorescence from adrenal tumors was also detected at variable levels of intensity. Cortisol-producing tumors had the highest fluorescence ratio of 3.01 ± 0.41. Confocal imaging localized autofluorescence to the cytosol, with the highest intensity in the zona reticularis followed by the zona fasciculata.

Conclusion: Normal and abnormal adrenal tissues possess natural NIR autofluorescence. Highest autofluorescence levels were associated with cortisol-producing tumors. Confocal imaging demonstrated the highest intensity in the zona reticularis. NIR cameras may have the potential to improve identification of adrenal tissue during surgery.

Key Words: adrenal tumor, adrenal glands, fluorescence, near-infrared, autofluorescence, zona reticularis

Abbreviations: AMF, average of the mean fluorescence; DAPI, 4′,6-diamidino-2-phenylindole; H&E, hematoxylin-eosin; ICG, indocyanine green; IF, immunofluorescence; IHC, immunohistochemistry; NIR, near infrared.

All tissues have some degree of autofluorescence, which is typically in the visible and ultraviolet range primarily from the aromatic rings of amino acids along with some enzyme cofactors such as NADH [1, 2]. The recent surge in fluorescence-guided surgery is almost exclusively in the near-infrared (NIR) range in part because of the relatively low autofluorescence of tissues in this spectrum [3, 4]. However, parathyroid glands (and to a much lower extent thyroid tissue) have been identified to have strong natural autofluorescence in the NIR range [5]. Using a probe to quantify the signal, the initial description found that parathyroid tissues have a nearly 7-fold higher autofluorescence intensity compared to thyroid tissue, with adjacent muscle, fat, and trachea having almost none. This discovery has led to improved intraoperative detection of parathyroid glands during thyroid and parathyroid surgery [6]. Furthermore, it has led to the US Food and Drug Administration approval of 2 real-time handheld devices to detect parathyroid based on their NIR autofluorescence [7]. The endogenous fluorophore in parathyroids and thyroid tissue has not been identified or localized at the cellular level [6]. To date, NIR native autofluorescence of other endocrine and neuroendocrine organs has not been well described.

Adrenalectomy is being performed at an increasing rate for various pathologic etiologies including benign, functional, and malignant tumors [8]. Despite the increased frequency of adrenalectomy, it remains a procedure relying heavily on the experience of the surgeon to distinguish the borders between the native adrenal gland and tumors from the surrounding retroperitoneal fat, vasculature, and adjacent viscera. Morbidities associated with adrenalectomy include bleeding, infection, injury to surrounding viscera and vasculature, diaphragmatic injury, as well as complications related to positive tumor margin and/or unintended partial adrenalectomy [9, 10]. Ultrasound, indocyanine green fluorescence (ICG),

Received: 7 April 2022. **Editorial Decision:** 7 August 2022. **Corrected and Typeset:** 13 September 2022

and methylene blue have been described as adjuncts to improve adrenal identification in situ [11-18]. All of these techniques have limitations. Specifically, for ICG, this includes nonspecific uptake related to tissue vascularity and need for injection, followed by proper detection timing [17].

We hypothesized that adrenal tissue possesses autofluorescence in the NIR spectrum similar to other endocrine organs. Herein we describe the novel characterization of autofluorescence in ex vivo human adrenal glands and further investigate its cellular localization in normal adrenal tissue and various types of adrenal tumor pathology.

Materials and Methods

Patients undergoing robotic adrenalectomy between January 1, 2020 and December 27, 2021 were included in this study. Informed consent was obtained from all patients. All work described was performed in accordance with the code of ethics of the World Medical Association for experiments involving humans under an institutional review board approved protocol (No. 2006C0047).

Near-Infrared Imaging

Patients did not receive any preoperative or intraoperative fluorescent dyes. After surgical excision of the adrenal gland in the operating room, the specimen was immediately imaged ex vivo for NIR autofluorescence. Imaging was performed using a commercially available handheld NIR camera (PDE-Neo II; Hamamatsu, Mitaka USA Inc) as described in a previously published work on parathyroid gland autofluorescence [19]. The NIR camera emits a wavelength of 760 nm using a light-emitting diode–excitation light with NIR capture of wavelengths ranging from 790 to 830 nm. Images of the gross specimen were obtained from all patients. The gross specimens frequently had a considerable amount of surrounding adipose tissue included with the tissue. To best preserve the specimen and any possible margins for pathologic evaluation, surrounding adipose was not removed from the gross specimens. To better delineate the areas of fluorescence and further define specific tissue and tumors, 6 normal adrenal- and 4 cortisol-producing tumor specimens were sectioned in the pathology laboratory and returned to the operating room to acquire additional images of sectioned or exposed tissues. A total of 22 images were taken in a darkroom with room lights off. Images were taken at a distance of 10 cm.

Post hoc analysis of the images was performed using Image J software (National Institutes of Health). Mean fluorescence of nontissue background, periadrenal fat, adrenal gland, and tumor tissue was recorded and used for comparison. Statistical analysis was performed with values normalized to the background (given the value of 1) and reported as an average of the mean fluorescent (AMF) signal ± SD.

Immunofluorescence

Microscopic analysis was performed with an Olympus FV3000 confocal microscope. To better define the subcellular location of the autofluorescence, tissues for immunofluorescence (IF) were stained with Phalloidin (F-actin) stain (Texas Red-X Phalloidin, ThermoFisher Scientific, T7471) to outline the cytoskeleton and Vectashield Hardset Antifade Mounting Medium with 4′,6-diamidino-2-phenylindole (DAPI; Vector Laboratories, H-1500-10) to define the nucleus. Tissues were fixed in 4% paraformaldehyde followed by embedding with 15% and 30% sucrose–phosphate-buffered solution, respectively. Tissues were placed in O.C.T, flash frozen on dry ice, and stored at –80 °C until use. Once frozen, tissues were sliced on a cryostat between 5 and 10 µm, depending on the structural integrity of tissues. Slices were placed on Fisherbrand Superfrost Plus Microscrope Slides (ThermoFisher Scientific, 12-550-15), followed by staining. Mouse lung and muscle were sourced from wild-type B6 mice and were used as negative controls.

Specific lasers were used to excite each stain as well as autofluorescence. Since the DAPI nuclear stain has an excitation-emission profile of 360 nm to 460 nm, the Alexa Fluor 405 laser was used, which excites at 405 nm. Likewise, Texas-Red has an excitation-emission profile of 591 nm to 608 nm, so the Alexa Fluor 568 laser was used, which excites as 561 nm. Given that autofluorescence is detected with an excitation source at 785 nm with a peak emission wavelength of 820 to 830 nm, we used an excitation laser at a wavelength of 752 nm (the closest available wavelength to 785 nm) to detect autofluorescence.

Immunohistochemistry

For light microscopic sections, tissues were fixed, placed in O.C.T., and sectioned in the same manner as IF samples. Sections were 5 to 10 µm thick, depending on the integrity of the tissue. Sectioned immunohistochemistry (IHC) samples were sent out for staining with routine hematoxylin and eosin (H&E) stains. Microscopic analysis was performed with an Olympus FV3000 confocal microscope.

Statistical analysis and graph generation were performed using GraphPad Prism (version 9.2.0). Images were separated into individual groups by tissue and pathology, as well as whether the images were from gross or sectioned tissue (gross normal adrenal, sectioned normal adrenal, and cortisol-producing tumor). The Kruskal-Wallis test was used to determine whether any statistical difference existed between the groups. Bonferroni correction was applied to correct for pairwise multiple comparisons type 1 error. Since there were 4 comparisons performed, the Bonferroni-corrected α value was 0.0125. Mann-Whitney tests were then performed, comparing each group to periadrenal fat AMF levels. *P* values calculated in each test matched. Nonparametric parameters were applied to account for nonnormal data distribution.

Results

A total of 22 patients underwent unilateral adrenalectomy for pheochromocytoma, primary aldosteronism, adrenocorticotropin-independent hypercortisolism, mild autonomous cortisol secretion, or a growing/suspicious mass. The cohort included 13 women and 9 men, with ages ranging from 34 to 79 years and a mean age of 55.7 ± 14.2. Patient body mass index ranged from 20 to 60.4 with a mean of 31.6 ± 9.5. Ex vivo gland weight ranged from 10.6 g to 153 g, with a mean weight of 36.3 ± 31.3 g (Table 1).

From the saved gross images, normal adrenal tissue was confidently identified in 20 of the 22 patients. In the other 2 specimens, there was too much overlying adipose to clearly identify normal adrenal tissue. In these 20 samples, surrounding periadrenal adipose tissue was also identified and analyzed for comparison with nontissue background

Table 1. Demographics

Sex	Age, y	BMI	Gland weight, g	Diagnosis
F	34	49	48.3	Cortical adenoma (hypercortisolism)
F	38	27.5	18.9	Cortical adenoma (hypercortisolism)
F	39	60.4	28.7	Cortical adenoma (hypercortisolism)
F	50	34.6	82.8	Cortical adenoma (hypercortisolism)
F	73	20	23.4	Cortical adenoma (hypercortisolism)
M	57	35.1	29.2	Cortical adenoma (hypercortisolism)
M	65	27.8	42	Cortical adenoma (hypercortisolism)
M	69	28.5	42.3	Cortical adenoma (hypercortisolism)
F	63	33	9.3	Mild autonomous cortisol secretion
M	52	30.7	20.9	Mild autonomous cortisol secretion
M	42	21	12.4	Primary aldosteronism
M	54	34.5	12	Primary aldosteronism
M	62	25.9	14.1	Primary aldosteronism
F	36	34.9	38.8	Growing mass
F	79	31.1	153	Suspicious mass
F	34	20.7	10.8	Pheochromocytoma
F	70	23.7	21.6	Pheochromocytoma
F	70	23.8	42.3	Pheochromocytoma
F	76	26.5	10.6	Pheochromocytoma
M	56	31.2	29.1	Pheochromocytoma
M	64	29.5	63	Pheochromocytoma
F	42	45.9	44.7	Vascular cyst

Abbreviations: BMI, body mass index; F, female; M, male.

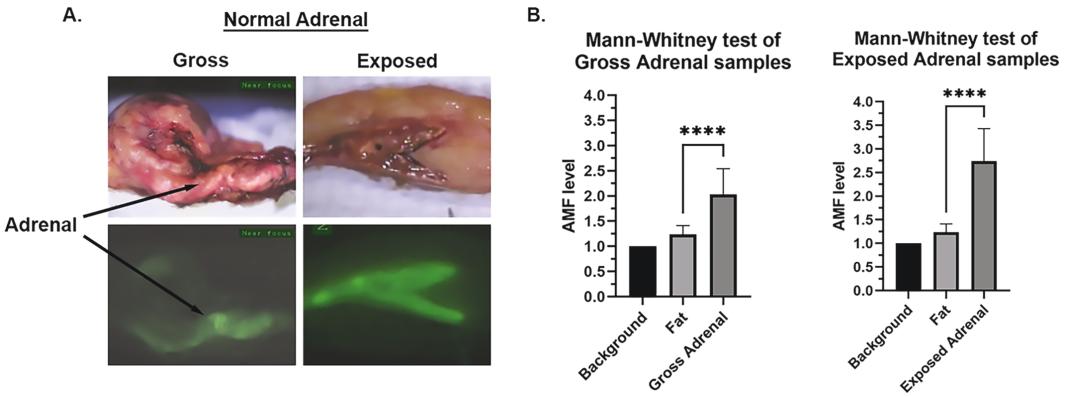

Figure 1. Near-infrared (NIR) imaging and quantitative analysis of normal human adrenal gland. A, Ex vivo normal human glands both in gross and exposed (sectioned) formats. Both glands show strong autofluorescence when compared to surrounding periadrenal adipose tissue, with exposed demonstrating stronger signal. B, Statistical analysis via Mann-Whitney shows significant difference in the average of the mean fluorescent (AMF) levels between both gross and exposed adrenal and periadrenal adipose AMF levels (*P* value: **** < .0001; gross n = 19, exposed n = 6).

set at 1. Periadrenal adipose tissue had an AMF ratio of 1.23 ± 0.18, and gross unsectioned normal adrenal tissue AMF was 2.03 ± 0.51. Six specimens with normal adrenal were sectioned to visualize the normal adrenal and any pathology more directly within the gland (Fig. 1A). AMF on these exposed internal surfaces was appreciably higher at 2.74 ± 0.44. Gross adrenal AMF and exposed adrenal AMF levels were significantly higher when compared to adipose tissue ($P < .0001$) (Fig. 1B).

These 22 functional and nonfunctional adrenal tumors included cortisol-producing tumors (10), pheochromocytomas (6), potential aldosterone-producing tumors (3), suspicious mass (2), and cystic (1) tumor(s) in which autofluorescence was measured. Of these gross images, clear identification of the tumor without overlying adipose was possible in cortisol-producing tumors (6), pheochromocytomas (3), potential aldosterone-producing tumors (1), suspicious mass (2), and cystic (1) tumor(s). Gross (unsectioned) tumor samples demonstrated variable levels of autofluorescence, with cortisol-producing tumor producing the largest AMF value (Fig. 2A and 2B). Pheochromocytomas and the vascular cyst had the lowest levels of autofluorescence, similar to that of adipose tissue. Of these tumors that underwent evaluation after sectioning, cortisol-producing tumors also displayed the highest level of autofluorescence with an AMF of 3.01 ± 0.41 in 4 exposed

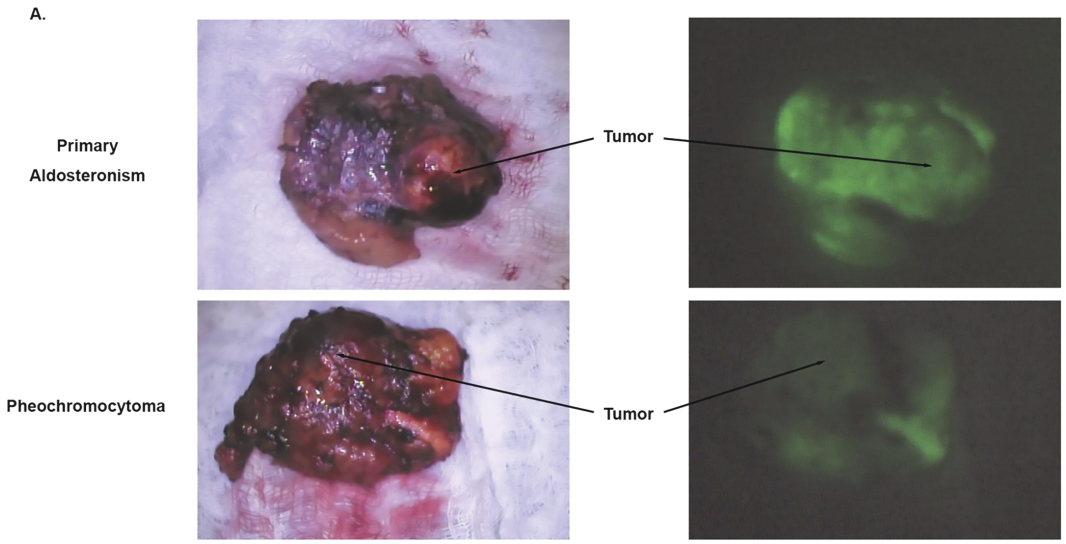

B.

Tumor Type	N	Mean ± SD
Cortisol Producing Tumor	6	2.43 ± 0.47
Primary Aldosteronism	1	1.8
Growing/suspicious mass	2	1.56 ± 0.20
Pheochromocytoma	3	1.19 ±0.05
Vascular Cyst	1	1.19
Background	1	1

Figure 2. Near-infrared (NIR) imaging of other tissue types along with associated average of the mean fluorescent (AMF) levels. A, NIR scans of both Primary aldosteronism and pheochromocytoma tissue samples. Both samples present regionalized but weaker tumor autofluorescence. B, Chart showing various other tissue samples and their associated AMF levels. Of the non–cortisol-producing tumor samples, the highest AMF level was found in primary aldosteronism with 1.8, which is much lower than the average gross cortisol producing tumor AMF level of 2.43 ± 0.47.

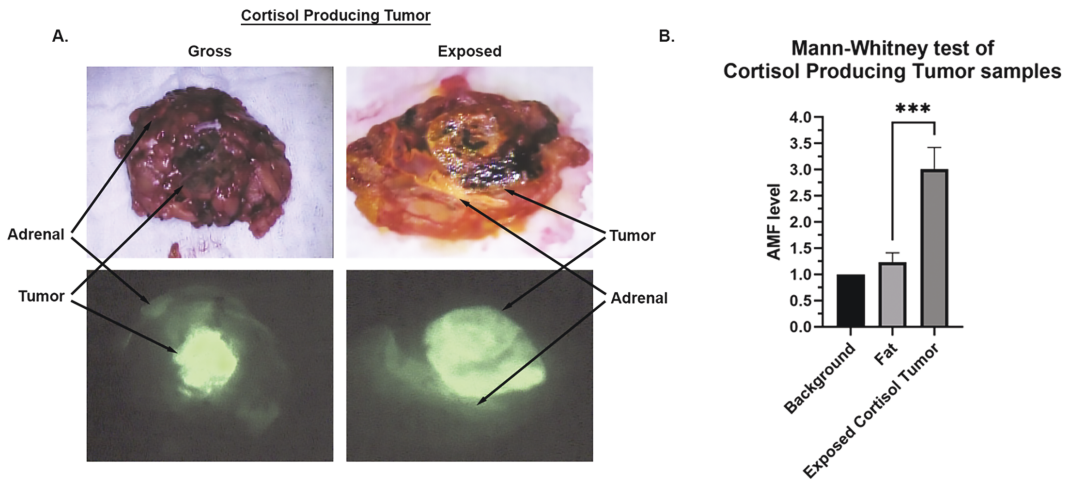

Figure 3. Near-infrared (NIR) imaging and quantitative analysis of exposed cortisol-producing tumor. A, Similar to normal adrenal samples, cortisol-producing tumor samples were examined both as gross and exposed (sectioned). Ex vivo cortisol-producing tumors presented similar strong autofluorescence both in gross and exposed samples. B, With exposed cortisol-producing tumor possessing the highest average of the mean fluorescent (AMF) level, statistical analysis via Mann-Whitney test shows exposed cortisol-producing tumor AMF levels to also be significantly greater than surrounding periadrenal adipose (*P* value: *** = .0001; n = 4).

surfaces, which was statistically significantly higher than background levels ($P < .0001$) (Fig. 3A and 3B).

To localize the adrenal autofluorescence at the cellular and tissue levels, adrenal tissues were examined by IF and IHC by confocal microscopy for DAPI nuclear staining to identify cells, and Texas-Red X Phalloidin (f-actin) for cytoskeletal staining. Confocal images consistently demonstrated autofluorescent signal within the cytoplasm of adrenal cells (Fig. 4A) using mouse muscle as a negative control (Fig. 4B).

Next, H&E-stained slides were used to better localize which region of the adrenal gland had the strongest fluorescence. Similar to IF, H&E-stained slides also localized fluorescence to an extranuclear region. Within the adrenal cortex, autofluorescence was most evident in the zona reticularis when

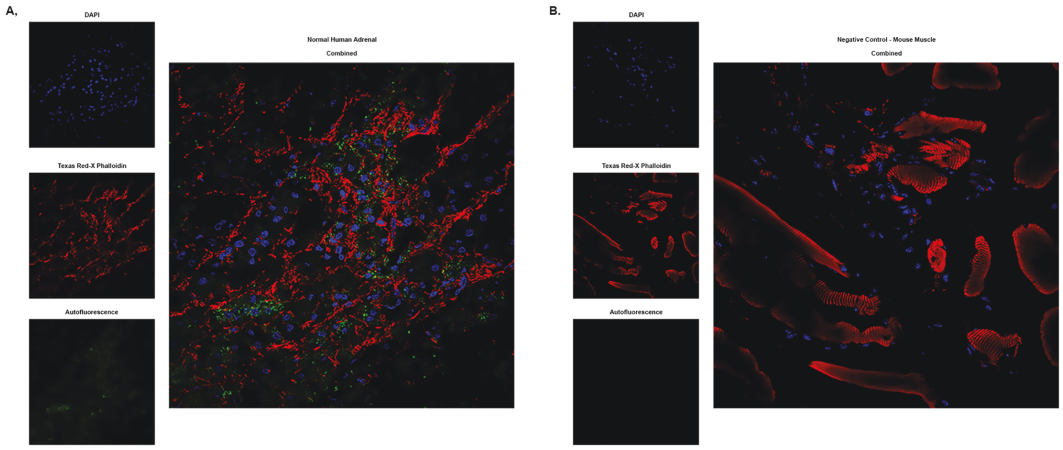

Figure 4. Confocal images. A, Normal human adrenal tissue expresses autofluorescence outside the nucleus. B, Mouse muscle was used as a negative control and shows no autofluorescence. Smaller images present DAPI, phalloidin, and autofluorescence separately. Combined images show how DAPI, phalloidin, and autofluorescence overlap. DAPI, 4′,6-diamidino-2-phenylindole.

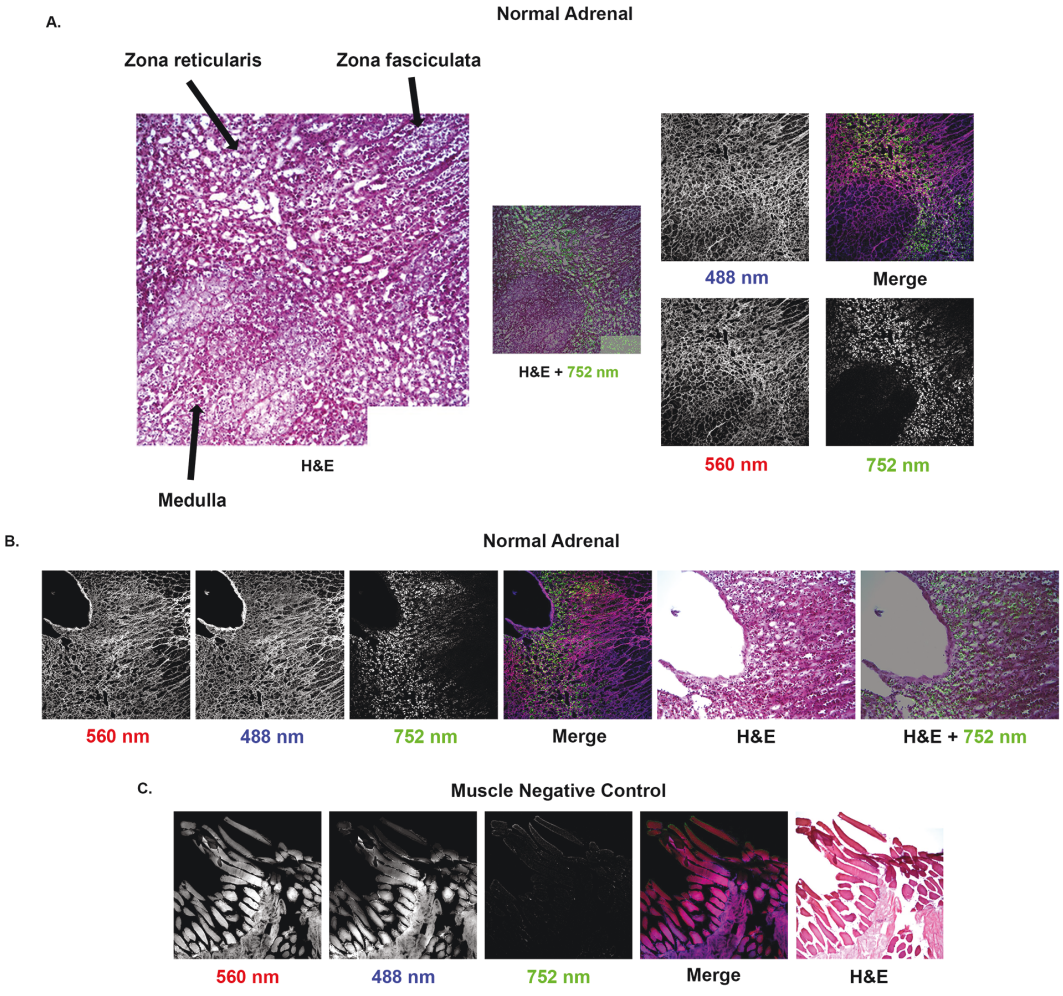

Figure 5. Immunohistochemistry (IHC) + confocal images. A, Normal adrenal sample presented. Images labeled 488 nm and 560 nm stand for the laser excitations used for autofluorescence of the hematoxylin-eosin (H&E) dye itself. These scans were included to show the tissue morphology; 752 nm is the excitation wavelength for endogenous autofluorescence from the adrenal tissue itself. The "Merge" image is a combination of 560 nm in red and 488 nm in blue. This created the purple coloration seen in the Merge image. Normal H&E was also included as well as a merged (H&E + 752 nm) image between the H&E and endogenous autofluorescence seen in green. B, Additional scans from the same tissue sample to show autofluorescence. Same labeling as described in A. A and B, Zona reticularis, zone fasciculata, and medulla are labeled on IHC, with autofluorescence localizing to the zona reticularis. The "fascicles," or bundles of the zona fasciculata, are present in the right-hand region of the tissue scans. The zona reticularis is found moving left, followed by the medulla on the left-hand region of the tissue scan. C, Human muscle is used as the negative control. Same labeling as described in A.

compared with other regions of the cortex (such as the zona fasciculata) and the adrenal medulla (Fig. 5A and 5B). Human muscle served as a negative control (Fig. 5C). Consistent with ex vivo analysis, normal adrenal tissue had lower autofluorescence compared with cortisol-producing tumors (Fig. 6).

Discussion

In the present manuscript, we demonstrate that adrenal tissue displays significant autofluorescence in the NIR spectrum. Autofluorescence was detected from the external surface of the gland and tissue from within the interior of the gland. Autofluorescence from both areas was significantly higher than adjacent adipose tissue. Adrenal tumors also demonstrated autofluorescence of varying intensity dependent on pathology and zonal origination, with cortisol-producing tumors having the highest signal (higher than normal adrenal tissue). The data serve as a "proof of principle" that autofluorescence might be useful to help guide adrenal surgery in the future.

Fluorescence-guided surgery is becoming a more commonly employed adjunct to help surgeons see anatomy and tissue perfusion, and locate pathology such as cancer [2]. Fluorescence requires an excitation light to penetrate tissue and be absorbed by the fluorophore, which subsequently emits a light at a different wavelength, which is detected with a camera. Important factors to maximize signal to background ratio include the penetrance of the excitation and emission light, as well as the scattering and absorption of light by the tissue. The NIR range is generally preferred for in vivo biologic imaging since these variables tends to be most favorable in this range, coupled with the fact that most tissue has very little autofluorescence in this range [3, 4]. ICG is an excellent NIR dye that has been used for in vivo imaging for decades but is a relatively nonspecific protein binder. While many targeted NIR dyes are being developed with several showing promise, autofluorescence is rarely used as the primary fluorescence source.

The source of endocrine tissue NIR autofluorescence is not known and has not been imaged at the cellular level [20]. Similar to parathyroid autofluorescence, we have found adrenal autofluorescence to last for days after tissue resection and does not appear to be affected dramatically by freezing and thawing, which allowed microscopic imaging many days later [21, 22]. Further studies are needed to determine if the adrenal fluorophore is the same as that seen in parathyroid and thyroid tissue. Confocal microscopy detects the endogenous adrenal fluorophore in the cellular cytoplasm. In addition, the highest autofluorescence occurs within the zona reticularis followed by the zona fasciculata with almost none seen in the adrenal medulla, demonstrating cell-type specificity within endocrine organs. These results correlate with the very low level of autofluorescence we report in pheochromocytomas at the gross level. A finding that needs further investigation is the relatively greater intensity of fluorescence from cortisol-producing tumors vs aldosterone-producing tumors given that aldosterone is primarily produced in the zona reticularis.

The discovery of autofluorescence in parathyroid, and to a lesser extent in thyroid tissues, led us to hypothesize that adrenal tissue might also autofluoresce in the NIR range. The ability to identify adrenal tissue may facilitate adrenal surgery, especially in those with abundant retroperitoneal adipose tissue. Differential autofluorescence of adrenal tissue compared to surrounding tissue may also allow for assurance that all adrenal tissue has been resected during total adrenalectomy, in addition to more directed dissection, thus potentially leading to improved outcomes after adrenalectomy and avoidance of continued presence or function of residual remnant tissue.

Several advances are required to make this finding of adrenal autofluorescence applicable to clinical practice. Additional studies are needed to define the optimal emission and excitation autofluorescence of adrenal tissue that need to be translated into usable camera systems. Real-time

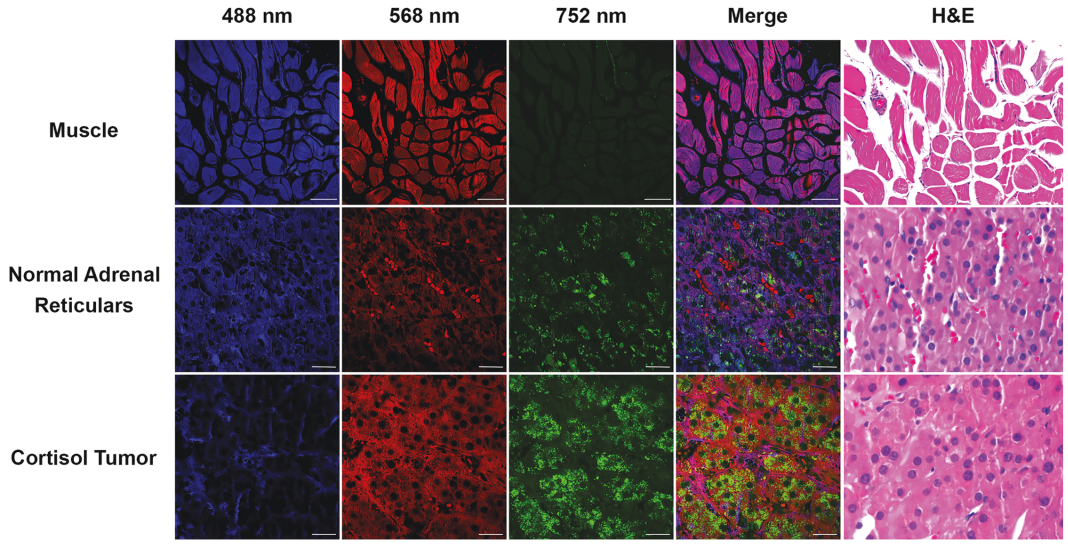

Figure 6. Tissue autofluorescence comparison. Panel comparing confocal scans of muscle (negative control), normal adrenal, and cortisol tumor. Similar to scans in Fig. 3, images labeled 488 nm and 560 nm stand for the laser excitations used for autofluorescence of the hematoxylin-eosin (H&E) dye itself. These scans were included to show the tissue morphology; 752 nm is the excitation wavelength for endogenous autofluorescence from the adrenal tissue itself. The 752 nm images were adjusted to the same dynamic range for proper signal intensity comparison. The "Merge" image is a combination of 560 nm in red, 488 nm in blue, and 752 nm in green. This created the purple coloration seen in the Merge image. Normal H&E was also included as well for reference.

quantification of autofluorescence in the operating room may also be helpful. Limitations of this study include the small number of samples, especially of some of the different tumor types. In addition, all work was performed ex vivo because of limitations in available camera technology to assess adrenal tissue in vivo. Nodules within resected adrenal glands of patients with primary aldosteronism were not stained for aldosterone synthase to prove the nodule was the source of excess aldosterone production. Whether AMF is affected by lack of perfusion and cell death is unknown, but similar to parathyroid NIR autofluorescence, adrenal NIR autofluorescence appears to fade very little over hours or days. Other factors affecting fluorescent intensity may not be appreciated and affect results.

Most currently used NIR imaging devices have been optimized for ICG, which likely has an emission and excitation profile different from that of natural fluorophore, so changing these aspects of the camera systems are likely needed. This includes the ability to apply the technology during both open and minimally invasive approaches. Although the Firefly NIR system available on certain robotic consoles visualizes ICG NIR signals well, the specifications of this system may need to be altered to image adrenal NIR autofluorescence. Finally, the molecular etiology and source of the native NIR fluorophore in adrenal tissues is unknown. Identifying the natural fluorophore may allow optimization of conditions to increase its intensity.

Conclusions

Adrenal tissue displays native NIR autofluorescence in freshly excised adrenal tissue compared to surrounding fat. Confocal imaging of adrenal tissue localized autofluorescence to within the cytoplasm, with the highest intensity originating from the zona reticularis. Cortisol-producing tumors have the highest level of autofluorescence. With additional research and continued development of NIR technology, this discovery opens the door to the potential for future clinical application.

Financial Support

This work was supported by the National Cancer Institute (grant Nos. P50CA168505, R01CA227847, R01CA240302 to M.D.R., and P30CA016058). We thank the Microscopy Shared Resource at the Ohio State University Comprehensive Cancer Center, Columbus, OH for microscope use and imaging.

Author Contributions

All authors were involved in the conception and design of the study, data analysis and interpretation, drafting or critically revising the document and provided final approval prior to submission.

Disclosures

The authors have nothing to disclose.

Conflict of Interest

John Phay is one of the inventors of a patent related to parathyroid autofluorescence imaging which was previously licensed to a company, AiBioMed, which is not a part of this study. None of the other authors have any conflicts of interest to declare related to this work.

Data Availability

Some or all data sets generated during and/or analyzed during the present study are not publicly available but are available from the corresponding author on reasonable request.

References

1. Lakowicz JR. *Principles of Fluorescence Spectroscopy*. 3rd ed. Springer; 2006:954.
2. Thammineedi SR, Saksena AR, Nusrath S, *et al*. Fluorescence-guided cancer surgery—a new paradigm. *J Surg Oncol*. 2021;123(8):1679-1698. doi:10.1002/jso.26469
3. Gioux S. Chapter 9: Fluorescence-guided surgery imaging systems: basics and advanced concepts. In: Hoffman R, Bouvet M, eds. *Strategies for Curative Fluorescence-Guided Surgery of Cancer. 1st ed.*; 2020;20:141-160.
4. Frangioni JV. In vivo near-infrared fluorescence imaging. *Curr Opin Chem Biol*. 2003;7(5):626-634. doi:10.1016/j.cbpa.2003.08.007
5. Paras C, Keller M, White L, Phay J, Mahadevan-Jansen A. Near-infrared autofluorescence for the detection of parathyroid glands. *J Biomed Opt*. 2011;16(6):067012. doi:10.1117/1.3583571
6. McWade MA, Paras C, White LM, *et al*. Label-free intraoperative parathyroid localization with near-infrared autofluorescence imaging. *J Clin Endocrinol Metab*. 2014;99(12):4574-4580. doi:10.1210/jc.2014-2503
7. Solórzano CC, Thomas G, Baregamian N, Mahadevan-Jansen A. Detecting the near infrared autofluorescence of the human parathyroid: hype or opportunity? *Ann Surg*. 2020;272(6):973-985. doi:10.1097/SLA.0000000000003700
8. Saunders BD, Wainess RM, Dimick JB, Upchurch GR, Doherty GM, Gauger PG. Trends in utilization of adrenalectomy in the United States: have indications changed? *World J Surg*. 2004;28(11):1169-1175. doi:10.1007/s00268-004-7619-6
9. Raffaelli M, De Crea C, Bellantone R. Laparoscopic adrenalectomy. *Gland Surg*. 2019;8(Suppl 1):S41-S52. doi:10.21037/gs.2019.06.07
10. Madani A, Lee JA. Surgical approaches to the adrenal gland. *Surg Clin North Am*. 2019;99(4):773-791. doi:10.1016/j.suc.2019.04.013
11. Manny TB, Pompeo AS, Hemal AK. Robotic partial adrenalectomy using indocyanine green dye with near-infrared imaging: the initial clinical experience. *Urology*. 2013;82(3):738-742. doi:10.1016/j.urology.2013.03.074
12. Obermeyer RJ, Knauer EM, Millie MP, Ojeda H, Peters MB Jr, Sweeney JF. Intravenous methylene blue as an aid to intraoperative localization and removal of the adrenal glands during laparoscopic adrenalectomy. *Am J Surg*. 2003;186(5):531-534. doi:10.1016/j.amjsurg.2003.07.011
13. Agcaoglu O, Kulle CB, Berber E. Indocyanine green fluorescence imaging for robotic adrenalectomy. *Gland Surg*. 2020;9(3):849-852. doi:10.21037/gs-2019-ra-06
14. Colvin J, Zaidi N, Berber E. The utility of indocyanine green fluorescence imaging during robotic adrenalectomy. *J Surg Oncol*. 2016;114(2):153-156. doi:10.1002/jso.24296
15. Sound S, Okoh AK, Bucak E, Yigitbas H, Dural C, Berber E. Intraoperative tumor localization and tissue distinction during robotic adrenalectomy using indocyanine green fluorescence imaging: a feasibility study. *Surg Endosc*. 2016;30(2):657-662. doi:10.1007/s00464-015-4256-0
16. DeLong JC, Chakedis JM, Hosseini A, Kelly KJ, Horgan S, Bouvet M. Indocyanine green (ICG) fluorescence-guided laparoscopic adrenalectomy. *J Surg Oncol*. 2015;112(6):650-653. doi:10.1002/jso.24057
17. Kahramangil B, Kose E, Berber E. Characterization of fluorescence patterns exhibited by different adrenal tumors: determining the

indications for indocyanine green use in adrenalectomy. *Surgery*. 2018;164(5):972-977. doi:10.1016/j.surg.2018.06.012
18. Dip FD, Roy M, Perrins S, *et al*. Technical description and feasibility of laparoscopic adrenal contouring using fluorescence imaging. *Surg Endosc*. 2015;29(3):569-574. doi:10.1007/s00464-014-3699-z
19. Squires MH, Jarvis R, Shirley LA, Phay JE. Intraoperative parathyroid autofluorescence detection in patients with primary hyperparathyroidism. *Ann Surg Oncol*. 2019;26(4):1142-1148. doi:10.1245/s10434-019-07161-w
20. Thomas G, McWade MA, Sanders ME, Solórzano CC, McDonald WH, Mahadevan-Jansen A. Identifying the novel endogenous near-infrared fluorophore within parathyroid and other endocrine tissues. *Biomed Opt*. 2016;PTu3A.5. doi:10.1364/OTS.2016.PTu3A.5
21. Moore EC, Rudin A, Alameh A, Berber E. Near-infrared imaging in re-operative parathyroid surgery: first description of autofluorescence from cryopreserved parathyroid glands. *Gland Surg*. 2019;8(3):283-286. doi:10.21037/gs.2018.12.05
22. Serra C. Persistence of autofluorescence of parathyroid glands submitted to heat, freeze and formalin. *Arch Clin Exp Surg*. 2020;9(1):18-21.